# Magnetocaloric properties, magnetic interactions and critical behavior in $Ho_6(Fe,Mn)Bi_2$ intermetallics

A. Herrero [a], A. Oleaga [a, *], A Salazar [a], A.V. Garshev [b], V. O. Yapaskurt [c], A.V. Morozkin [b]

[a] Departamento de Física Aplicada I, Escuela de Ingeniería de Bilbao, Universidad del País Vasco UPV/EHU, Plaza Torres Quevedo 1, 48013 Bilbao, Spain
[b] Department of Chemistry, Moscow State University, Lenisnkie Gory, House 1, Building 3, Moscow, GSP-2, 119991, Russia
[c] Department of Petrology, Geological Faculty Moscow State University, Leninskie Gory, Moscow, 119991, Russia

## ABSTRACT

Four polycrystaline $Fe_2P$-type $Ho_6(Fe,Mn)Bi_2$ intermetallic compounds (space group $P\bar{6}2m$, No. 189, *hP*9) have been studied using magnetic techniques in order to explore their ability as magnetocaloric materials, and study the critical behavior of the paramagnetic (PM) to ferromagnetic (FM) transitions to obtain a deeper understanding of the range of the magnetic interactions. The obtained critical exponents $\beta$, $\gamma$ and $\delta$ for the four compounds studied ($Ho_6MnBi_2$, $Ho_6FeBi_2$, $Ho_6(Mn_{0.5}Fe_{0.5})Bi_2$, $Ho_6(Mn_{0.75}Fe_{0.25})Bi_2$) point to long-range order interactions, as they are close to those of the Mean Field Universality class. All of the compounds show relevant magnetocaloric properties over a very broad temperature range, limited by the PM-FM transition and a spin-reorientation one, well separated in all cases. They present very high values of the refrigerant capacities (from 520 J/kg to 709 J/kg at 5 T), good magnetic entropy changes (from 3.4 to 5.7 J/(kgK) at 5 T), and a flat and wide temperature span for the working temperature range (nearly 200 K for $Ho_6MnBi_2$, 80 K for $Ho_6FeBi_2$ at 5T). The change in properties with composition proves that the magnetocaloric properties can be tuned in $Fe_2P$-type compounds to accommodate different refrigeration applications. Finally, the magnetocaloric scaling laws have been successfully tested and universal curves for the magnetic entropy change have also been obtained in the PM-FM transition region.

**Keywords:** Magnetocaloric effect; Rare earth compound; Magnetic properties; Spin-ordering; Critical behavior

*Corresponding author; E-mail: alberto.oleaga@ehu.es

## 1. Introduction

The need to introduce environmentally friendly technology in the energy field has led to huge advances in the research and development of new refrigeration technology based on the magnetocaloric effect, with the aim of replacing the classical gas compressor-expansion cycles [1-3]. To this end, a thorough collective effort is being done in pursuit of magnetocaloric materials which present suitable properties for technological applications in different temperature ranges. Though giant magnetocaloric effects have been obtained for several materials which present first-order magnetic phase transitions, the hysteresis commonly present and the thin temperature span of the magnetocaloric effect limit their application; besides, in these materials the magnitude of the magnetocaloric effect has been generally indirectly evaluated by means of the magnetic entropy change $\Delta S_M$, which has been incorrectly calculated in many cases, due to an improper use of the Maxwell equation

$$\Delta S_M(\mathrm{T},\Delta\mathrm{H}) = \mu_0 \int_{H_i}^{H_f} \left(\frac{\partial M}{\partial T}\right)_H dH \qquad (1)$$

($M$ stands for magnetization, $T$ for temperature and $H$ for magnetic field), generating spourious peaks in $\left|\Delta S_M\right|$, which imply that the magnitude of the effect is not as huge as assumed [4-8]. On the other hand, the magnetocaloric materials with second order magnetic phase transitions present values for the magnetic entropy change or the adiabatic temperature change not so high but without hysteresis and with a wider temperature span [2]. In all cases, the indirect methods of evaluation are the commonest as they are at the disposal of most labs, which is the reason why the magnetic entropy change is generally taken and compared as the indicator of the relevance of the magnetocaloric effect, instead of a direct evaluation of the adiabatic temperature change.

The quest is now focused on finding magnetocaloric materials with the following properties: no thermal or magnetic hysteresis in the magnetic transition, a wide temperature span in the temperature region of interest, a high magnetic entropy change, as flat as possible over the working temperature range, and a high refrigerant capacity. Concerning the temperature region of interest, a big effort is being done in developing magnetocaloric materials which can work at (or close to) room temperature, where different families have been found to show interesting characteristics (Gd and its

compounds, Heusler alloys, manganites, etc. [9-16]), but there is also a growing interest in the gas liquefaction ranges, with different Laves phases ($R$Co$_2$, $R$Al$_2$ , $R$ = Ho, Dy, Er and derivatives), $R$FeSi ($R$=Dy, Er, Tb and mixed rare earths), or Gd$_5$(Si,Ge)$_4$ showing competitive properties [2, 17]. Finally, there are also innovative trends in the production of multi-component compounds which might give a wider temperature range with a constant value of the magnetic entropy change, mixing intermetallic materials, such as (Tb$_{1-x}$Dy$_x$)FeSi (x from 0 to 1) [18] or $R_2T_2X$ ($R$ = Gd-Tm; $T$ = Cu, Ni, Co; $X$ = Cd, In, Ga, Sn, Al) [19].

Ternary intermetallic compounds of very different sort are being synthesized in this research field as the combination of rare earths and transition metals give interesting magnetic properties, locating the magnetic transitions at varied temperatures, depending on the particular compositions. In this paper we are focusing our attention on the Fe$_2$P-type Ho$_6$MnBi$_2$, Ho$_6$FeBi$_2$ and the intermediate compounds Ho$_6$(Mn$_{0.5}$Fe$_{0.5}$)Bi$_2$, Ho$_6$(Mn$_{0.75}$Fe$_{0.25}$)Bi$_2$. Ho, on its own, has been found to present magnetocaloric properties with maximum values at $T_N$ = 132 K and at $T_C$ = 20 K, [1, 20, 21]. The magnetocaloric properties of different compounds containing Ho have already been studied (see the review work by Franco *et al* [2]) and we have selected the intermetallics mentioned above as the magnetic properties already studied of Ho$_6$MnBi$_2$ and Ho$_6$FeBi$_2$ make them specially interesting [22, 23]: both of them present a paramagnetic to ferromagnetic transition (PM-FM) followed by a spin reorientation transition at a much lower temperature, and the difference between the Curie temperatures in the sample with Mn and the sample with Fe is higher than 130 K. So there is the possibility of having two magnetocaloric effects in the samples covering a wide temperature range which could be shifted varying the stoichiometry and maybe obtaining a sustained value of the magnetic entropy change in the whole range. A recent magnetocaloric study on Ho$_6T$Te$_2$ ($T$=Fe, Co) has shown the ability of this family of ternary compounds to present this kind of properties [24], as it was already found in Gd$_6$CoTe$_2$ [25]. Therefore, the aim of this work is to carry out a thorough study on the magnetocaloric properties of Ho$_6$(Mn,Fe)Bi$_2$ intermetallics, including the study of the critical exponents of the paramagnetic to ferromagnetic transition, which will give the possibility of checking the scaling equation for the maximum of the magnetic entropy change

$$\Delta S_M^{pk} \propto H^{1+(1/\delta)(1-1/\beta)} \qquad (2)$$

where $\beta$ and $\delta$ are the critical parameters associated to the spontaneous magnetization and the critical isotherm, respectively.

$$M_S(T) \sim |t|^{\beta} \qquad (T < T_C), \tag{3}$$

$$M(H) \sim H^{1/\delta} \qquad (T = T_C), \tag{4}$$

and $t = (T-T_C)/T$ the reduced temperature [26-28]. The knowledge of the critical parameters will also allow us to get a deeper insight in the physics of the magnetic properties, including the extent of the magnetic interactions, depending on which universality class they belong to [29]. To this end, the full set of critical parameters ($\beta$, $\gamma$, $\delta$) will be obtained, adding to the previous equations the one for the inverse of the initial susceptibility

$$\chi_0^{-1}(T) \sim |t|^{\gamma} \qquad (T > T_C), \tag{5}$$

with the magnetic equation of state which must be fulfilled in the critical region

$$M(H, t) = |t|^{\beta} f_{\pm}(H/|t|^{\beta+\gamma}) \tag{6}$$

where $f_-$ and $f_+$ are regular analytic functions for $T < T_C$ and $T > T_C$, respectively. Table 1 contains the theoretical values of the magnetic critical exponents for the most relevant universality classes.

Table 1. Main universality classes for different magnetic systems.

| ***Universality class*** | ***β*** | ***γ*** | ***δ*** | ***Order of the magnetic interactions & Spin arrangement*** |
|---|---|---|---|---|
| Mean-field Model | 0.5 | 1.0 | 3.0 | Long-range order |
| 3D-Ising | 0.3265 | 1.237 | 4.79 | Short-range order<br>Uniaxial anisotropy |
| 3D-Heisenberg | 0.365 | 1.386 | 4.80 | Short-range order<br>Isotropy |

## 2. Materials and methods

Alloys with a total mass of 2 g were prepared by arc-melting in an electric arc furnace (90 V, 150 A) under argon (99.992 vol. %) using a non-consumable tungsten electrode and on a water-cooled copper hearth. Pieces of holmium (99.9 wt. %), iron, manganese (99.95 wt. %) and bismuth (purity 99.99 wt.%) were used as starting components. A titanium button was used as a getter during arc-melting and the alloys were remelted three times. The arc-melted samples were wrapped into nickel foil and sealed in silica ampoules, evacuated and back filled with argon to 0.3 atm at room temperature. The samples were annealed at 1070 K (± 2 K) for 300 hours, then quenched in ice-water bath.

Phase analysis of the alloys was carried out using X-ray diffraction and energy dispersive X-ray spectroscopy microprobe elemental analysis (EDS). The X-ray powder data (XRD) were obtained by using a diffractometer Rigaku D/MAX-2500 (CuKα, 2θ of 10-80°, 0.02° step, $I_{max}/I_{bgr}$ ~ 50). An INCA-Energy-350 X-ray EDS spectrometer (Oxford Instruments) on a Jeol JSM-6480LV scanning electron microscope (SEM) (20 kV accelerating voltage, 0.7 nA beam current and 50 μm beam diameter, microprobe size ~ 10 nm) was employed to perform quantitative elemental analysis. Signals averaged over three points per phase gave estimated standard deviations of 0.5 at.% for holmium (measured by L-series lines), 1 at.% for Mn, Fe and Bi (measured by K-series lines).

The unit cell data were derived from powder X-ray data using the Rietan-program [30] in the isotropic approximation at room temperature.

A VSM (Vibrating Sample Magnetometer) by Cryogenic Limited has been used to perform magnetization ($M$) measurements under external applied magnetic fields $H_a$ in the range of 0 to 7 T. Isotherms have been collected from low temperatures (~ 6 K) to temperatures well above the corresponding Curie temperature ($T_C$) for each sample. A step of $\Delta T$ = 1 K between consecutive isotherms has been used around $T_C$ in order to properly cover this region for the critical behavior study. For a correct evaluation of both the scaling analysis and the magnetocaloric effect, the demagnetization field has to be taken into account [31, 32] and, therefore, the applied magnetic field $H_a$ has been corrected and the internal field obtained according to the relation $H_i = H_a - NM$, where $M$ is the measured magnetization and $N$ the demagnetization factor. Zero–field *ac* susceptibility measurements have been used to obtain $N$ from the maximum value of the peak of this magnitude ($N = 1/\chi_{max}$) [33, 34] and the so obtained values are collected in

Table 2. The magnetic susceptibility was measured with AC Measurement System Option in PPMS (Physical Properties Measurement System) by Quantum Design.

Table 2. Demagnetization factors experimentally obtained

| Material | $N$ (Oe/g emu) |
|---|---|
| $Ho_6MnBi_2$ | 69.29 |
| $Ho_6(Mn_{0.75}Fe_{0.25})Bi_2$ | 78.96 |
| $Ho_6(Mn_{0.5}Fe_{0.5})Bi_2$ | 97.59 |
| $Ho_6FeBi_2$ | 84.10 |

## 3. Experimental results and discussion

The X-ray powder analysis showed that the $Ho_6Mn_xFe_{1-x}Bi_2$ (x = 0, 0.5, 0.75, 1) ('$Ho_{65.7(8)}Fe_{11.4(8)}Bi_{22.9(9)}$', '$Ho_{66.5(6)}Mn_{5.3(8)}Fe_{6.5(7)}Bi_{21.7(5)}$', '$Ho_{67.1(6)}Mn_{7.0(7)}Fe_{4.3(6)}Bi_{21.6(4)}$' and '$Ho_{67.2(5)}Mn_{11.1(4)}Bi_{21.7(4)}$' compositions from microprobe analysis, respectively) crystallize in the $Fe_2P$-type structure (space group $P\bar{6}2m$, No. 189, *hP*9). The refined unit cell data and atomic positions are given in Table 3. The substitution of Fe for Mn is followed via increasing of unit cell volume and anisotropic distortion of unit cell (increasing of *c*/*a* ratio) from $Ho_6FeBi_2$ to $Ho_6MnBi_2$. Fig. 1 shows the Rietveld refinement and SEM photograph of $Ho_6(Mn_{0.5}Fe_{0.5})Bi_2$, as an example.

Due to diffusion way of synthesis of these polycrystals, the alloys contain an admixture of $Yb_5Sb_3$-type $Ho_5(Fe,Mn)_{\sim 0.5}Bi_{\sim 2.5}$ phases (~10 wt. % for $Ho_6FeBi_2$, ~10% for $Ho_6(Mn_{0.5}Fe_{0.5})Bi_2$, ~12% for $Ho_6(Mn_{0.75}Fe_{0.25})Bi_2$ and ~14% for $Ho_6MnBi_2$). This admixture exhibits ferromagnetic ordering around 40 K (see e.g. [35]) and it shows a small influence for the resulting magnetic properties, as will be discussed later.

Table 3. Unit cell data of $Fe_2P$-type $Ho_6Mn_xFe_{1-x}Bi_2$ compounds [a-] (space group $P\bar{6}2m$, No. 189, *hP*9).

| **Compound** | ***a*** (nm) | ***c*** (nm) | ***c/a*** | $V$ (nm$^3$) | $x_{Ho1}$ | $x_{Ho2}$ | $R_F$ (%) |
|---|---|---|---|---|---|---|---|
| $Ho_6MnBi_2$ | 0.81822(5) | 0.42609(2) | 0.520752 | 0.247043 | 0.6069(6) | 0.2364(6) | 3.2 |
| $Ho_6(Mn_{0.75}Fe_{0.25})Bi_2$ | 0.81971(5) | 0.42265(2) | 0.515609 | 0.245942 | 0.6079(6) | 0.2342(5) | 3.6 |
| $Ho_6(Mn_{0.5}Fe_{0.5})Bi_2$ | 0.81983(5) | 0.42096(2) | 0.513472 | 0.245030 | 0.6052(6) | 0.2348(6) | 3.4 |
| $Ho_6FeBi_2$ | 0.82220(6) | 0.41816(3) | 0.508587 | 0.244809 | 0.6049(6) | 0.2340(6) | 3.7 |

[a-] Ho1 (3*g*) [$x_{Ho1}$, 0, 1/2], Ho2 (3*f*) [$x_{Ho2}$, 0, 0], $Mn_{1-x}Fe_x$ (1*b*) [0, 0, 1/2], Bi (2*c*) [1/3, 2/3, 0].

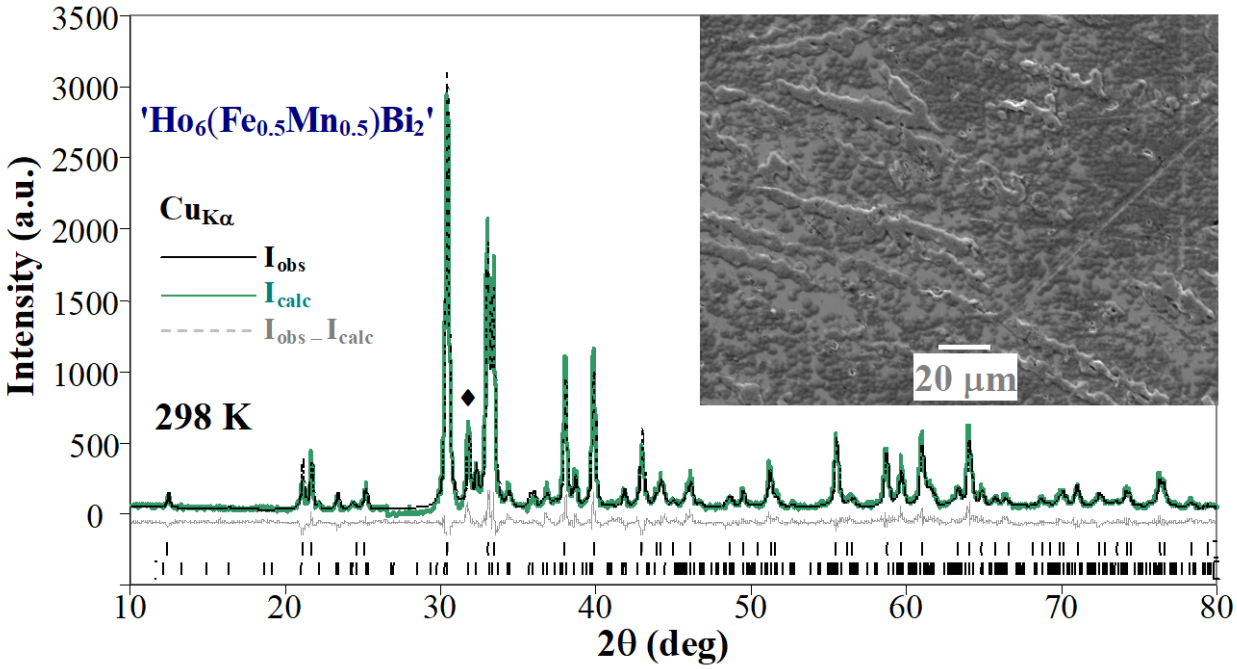


Fig. 1. Rietveld refinement of the X-ray powder pattern and SEM photo of the '$Ho_6Fe_{0.5}Mn_{0.5}Bi_2$': alloy contains ~90 wt.% of $Fe_2P$-type $Ho_6(Fe_{0.5}Mn_{0.5})Bi_2$ ($R_F$ = 3.4 %) ($Ho_{66.5(6)}Fe_{6.1(8)}Mn_{5.4(8)}Bi_{22.0(4)}$ from X-ray spectral analysis: dark-grey phase) and ~10 wt. % of $Yb_5Sb_3$-type $Ho_5Fe_{0.4}Mn_{0.1}Bi_{2.5}$ ($R_F$ = 3.0 %) ($Ho_{63.7(8)}Fe_{4.5(9)}Mn_{1.0(6)}Bi_{30.8(5)}$ from X-ray spectral alalysis: white phase). The first and second rows of ticks refer to the diffraction peaks of $Ho_6(Fe_{0.5}Mn_{0.5})Bi_2$ and $Ho_5Fe_{0.4}Mn_{0.1}Bi_{2.5}$, respectively. The strongest peak of admixture $Yb_5Sb_3$-type $Ho_5Fe_{0.4}Mn_{0.1}Bi_{2.5}$ is marked in **Figure** (♦). The grey phase in SEM photo is the surface oxide's film of $Fe_2P$-type $Ho_6(Fe_{0.5}Mn_{0.5})Bi_2$.

Fig. 2a shows the evolution of the magnetization per unit mass as a function of temperature while Fig. 2b presents the real part of the *ac* susceptibility, in order to place the transitions with precision using the maxima. They all share similar shapes: from room temperature, with decreasing temperature a first paramagnetic PM to ferromagnetic FM transition takes place at $T_C$ (203 K, 150 K, 128 K, 72 K for $Ho_6MnBi_2$, $Ho_6(Mn_{0.75}Fe_{0.25})Bi_2$, $Ho_6(Mn_{0.5}Fe_{0.5})Bi_2$ and $Ho_6FeBi_2$, respectively); then, as temperature keeps on decreasing, the magnetization is still increasing until a second transition takes place, $T_m$, due to spin reorientation [22, 23], whose value is marked by the lower temperature maxima in the susceptibility (52 K, 30 K, 26 K and 31 K, respectively). $Ho_6MnBi_2$ shows the highest magnetization until the lower temperature transition takes place in $Ho_6(Mn_{0.75}Fe_{0.25})Bi_2$, when the latter compound surpasses the magnetization value of the former, presenting the highest value at low temperatures. In

the susceptibility measurements, a small shoulder can be traced for $Ho_6MnBi_2$ at 44 K and $Ho_6(Mn_{0.75}Fe_{0.25})Bi_2$ at 41 K, probably due to the ordering of the $Yb_5Sb_3$-type admixture phase, while it is not seen in the other two, where the amount of this phase is smaller.

Comparing the results from Fig. 2 to those presented in Table 3, it can be seen that the change in the Curie temperature is related to the change in the cell parameters, which implies it is linked to the separation between rare earth ions (see Fig. 3). This has already been observed in Ho-based intermetallic compounds [22] as well as in Gd-based ones [36]. The transition metals do not have a net magnetic moment in the $R_6TX_2$ family, in general [36, 37] and this has been proved, in particular, for $Ho_6MnBi_2$ and $Ho_6FeBi_2$ [23]. This implies that they can all be considered as rare-earth intermetallics, with magnetism only due to *4f-4f* coupling, so that the magnetism could be explained on the basis of the RKKY model. The problem arises when trying to explain the cases in which the intermetallic has a much higher $T_C$ than the rare earth metal, as is the case for Ho-based intermetallics (Ho presents ferromagnetic ordering at $T_C$ = 20 K). It is generally considered that, apart from the distortion of the unit cell, hybridization between electronic orbitals of the rare earth and the other ions in the compound increases the exchange interaction in intermetallics so that the Curie temperatures are raised [1, 36, 38]. In particular, Mn has a very special effect as it strongly raises the ordering temperature, much more than other transition metals [22]. The particular mechanism through which this is obtained is still to be found.

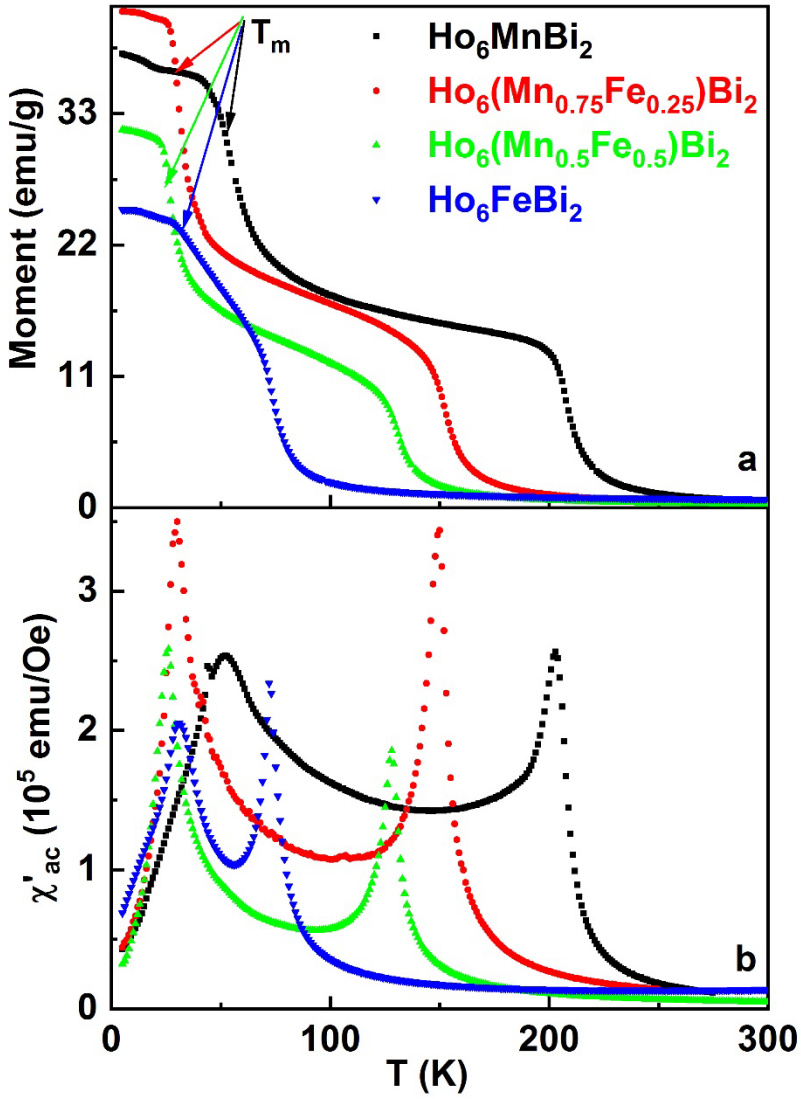


Fig 2. a) Magnetic moment as a function of temperature in field-cooled (FC) mode with applied field H = $10^3$ Oe; b) real part of the *ac* susceptibility at $f$ = 100Hz.

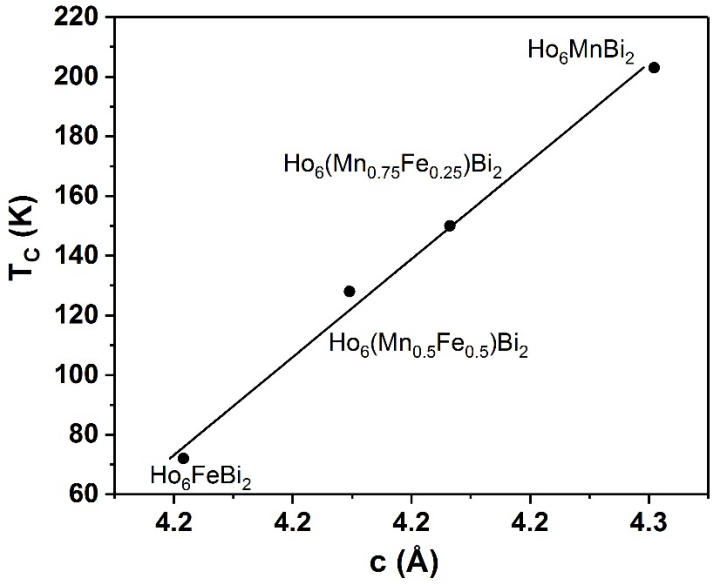


Fig. 3. Dependence of the Curie temperature with the *c*-axis.

### 3.1. Critical behavior.

As stated in the introduction, we have proceeded with the study of the universality class to which the second order PM-FM transition belongs by extracting the critical exponents from magnetic measurements, using in each case the isotherms in the region around $T_C$ (172-232 K for $Ho_6MnBi_2$, 126-175 K for $Ho_6(Mn_{0.75}Fe_{0.25})Bi_2$, 106-146 K for $Ho_6(Mn_{0.5}Fe_{0.5})Bi_2$ and 50-92 K for $Ho_6FeBi_2$). These regions are far enough away from the low temperature transitions so that the results obtained from this study will be reliable as there is no overlapping with other critical regions.

In order to simplify the notation, in what follows $H$ will be used instead of $H_i$ to represent the internal field. The first step is to represent for every sample the well known Arrot Plot, where $M^2$ versus $H/M$ is plotted. All the samples present the same behaviour and it is illustrated by Fig. 4a for the particular case of $Ho_6MnBi_2$.

It can be seen that the slopes are positive, which according to the Banerjee criterion [39] confirms the second order character of these transitions and therefore the applicability of the critical behavior theory. That graph implies a particular selection of critical exponents ($\beta = 0.5$, $\gamma = 1$) which corresponds to the Mean Field universality class (see Table 1). If the PM-FM transition belonged to this class, in Fig. 4a the isotherms at high fields should be straight lines, parallel to each other. It can be clearly seen that they are nearly straight lines but parallelism is not too good. Therefore, we have turned our

attention to the so called Modified Arrot Plots (MAP), representing $M^{1/\beta}$ as a function of $(H/M)^{1/\gamma}$ for other relevant universality classes, such as 3D-Heisenberg ($\beta$ = 0.365, $\gamma$ = 1.386) and 3D-Ising ($\beta$ = 0.3265, $\gamma$ = 1.237), which are represented in Fig. 4b and 4c. It is evident that the Mean Field critical exponents give the most parallel and straight lines among the tested models for all the materials. As the parallelism is not perfect we have tested different sets of parameters close to the Mean Field model and then followed the well known iteration procedure by which the starting critical exponents are refined [40, 41]. Fig. 4d contains the starting values before the iteration procedure for $Ho_6MnBi_2$. A linear extrapolation from high field data on the MAP has been used to extract the $(M_S)^{1/\beta}$ and $(\chi_0^{-1})^{1/\gamma}$ values as the interception with Y and X axes, respectively. Once $M_S(T)$ and $\chi_0^{-1}(T)$ have been obtained they are fitted to Eqs. (3) and (5) to obtain new values of $\beta$ and $\gamma$, which are then used for another iteration until the values converge and good parallel, straight lines, are obtained in the MAP. Fig. 5 shows the final values of $M_S(T)$ and $\chi_0^{-1}(T)$ and their corresponding fittings as a function of temperature for all the samples. All the critical exponents and temperatures are collected in Table 4. The final obtained $\beta$ values are higher than the corresponding to the MF model, where $\beta$ = 0.5, in every case getting far from any other universality class, while $\gamma$ is also slightly higher than 1 (the corresponding value in the MF model) except in the $Ho_6FeBi_2$ sample where it is slightly lower. This means that short range magnetic interactions are not active in these compounds but long-range ones.

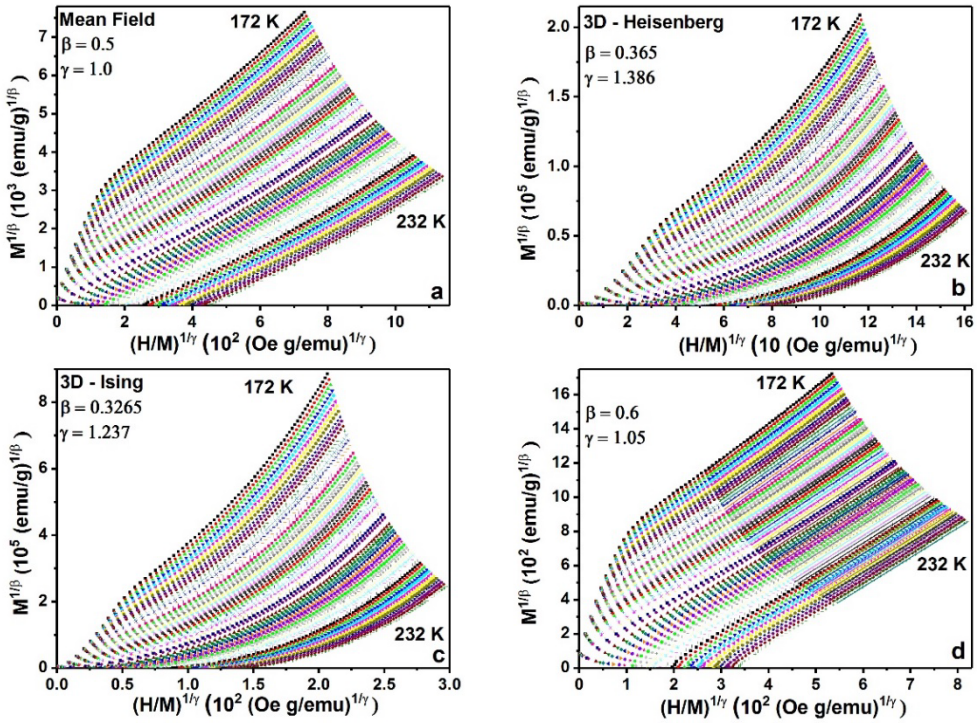


Fig. 4. a) Arrot plot, corresponding to the Mean Field univerality class parameters; b) Modified Arrot Plot for the 3D-Ising class; c) Modified Arrot Plot for the 3D-Heisenberg class ; d) Modified Arrot Plot for selected critical parameters as starting point for their refinement. All of them for $Ho_6MnBi_2$.

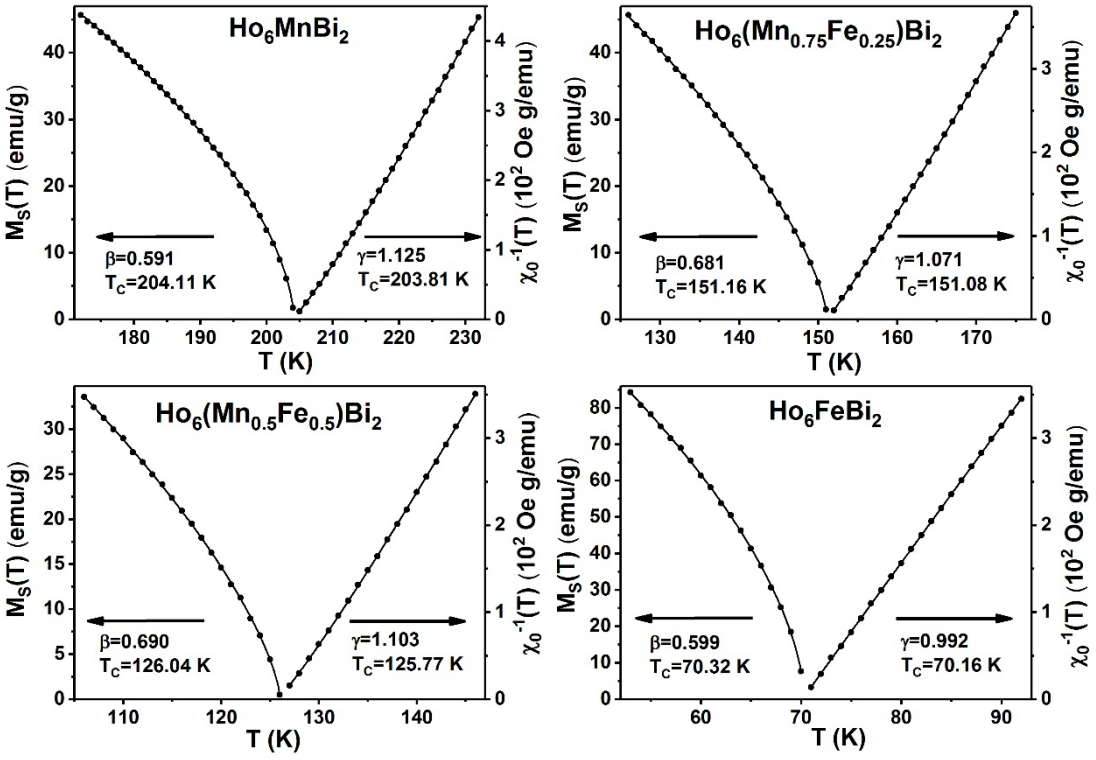


Fig. 5. Spontaneous magnetization (left) and inverse of initial susceptibility (right) vs. temperature for the four compounds as obtained from the optimized Modified Arrot Plot. The solid curves correspond to the fits to Eq. (3) and (5), as explained in the text.

The parameters $\beta$, $\gamma$ and $T_C$ have also been obtained by the widely used Kouvel Fisher method (KF) for the four samples. This method assesses that both $Ms(dM_S/dT)^{-1}$ and $\chi_0^{-1}(d\chi_0^{-1}/dT)^{-1}$ have a linear dependency with respect to $T$, with slopes equal to $1/\beta$ and $1/\gamma$, respectively [42]. The Curie temperature is given by the interception of the straight fitted lines on the temperature axis. The Kouvel Fisher plots, their corresponding fittings and the retrieved parameters are shown in Fig. 6. As can be seen from Table 4 there is a good agreement between the exponents obtained by means of the Modified Arrot Plots and the Kouvel-Fisher method, confirming the robustness of the results.

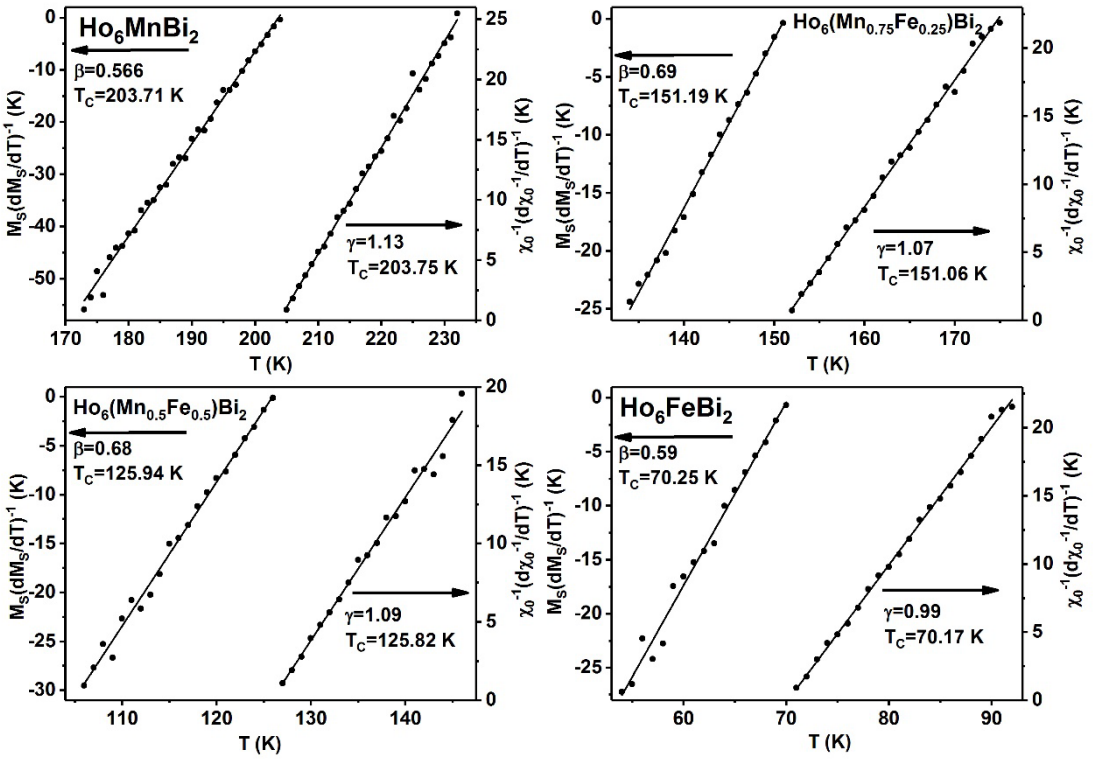


Fig. 6. Kouvel-Fisher plot of spontaneous magnetization (left) and inverse of initial susceptibility (right) for the four compounds. The straight lines are linear fits, from which $T_C$ and the critical exponents are obtained.

The last magnetic critical exponent, $\delta$, is associated to the critical isotherm by Eq. (4) and can therefore be obtained experimentally. Fig. 7 shows the magnetization as a function of the internal field for the four samples at their corresponding critical temperatures (204 K for $Ho_6MnBi_2$, 151 K for $Ho_6(Mn_{0.75}Fe_{0.25})Bi_2$, 126 K for $Ho_6(Mn_{0.5}Fe_{0.5})Bi_2$, and 70 K for $Ho_6FeBi_2$) in a log-log scale. It can be seen that the experimental data lies on good straight lines whose slopes give the value of $\delta$.

Scaling laws also give a mathematical relation between the different magnetic critical exponents that have been discussed so far [29]:

$$\delta = 1 + \gamma/\beta \quad (7)$$

This equation can be used to obtain $\delta$ from the $\beta$ and $\gamma$ values previously obtained through MAP and Kouvel Fisher methods. The values given by Eq. (7) are very close to those obtained directly from the critical isotherms. The results can be compared in Table 4.

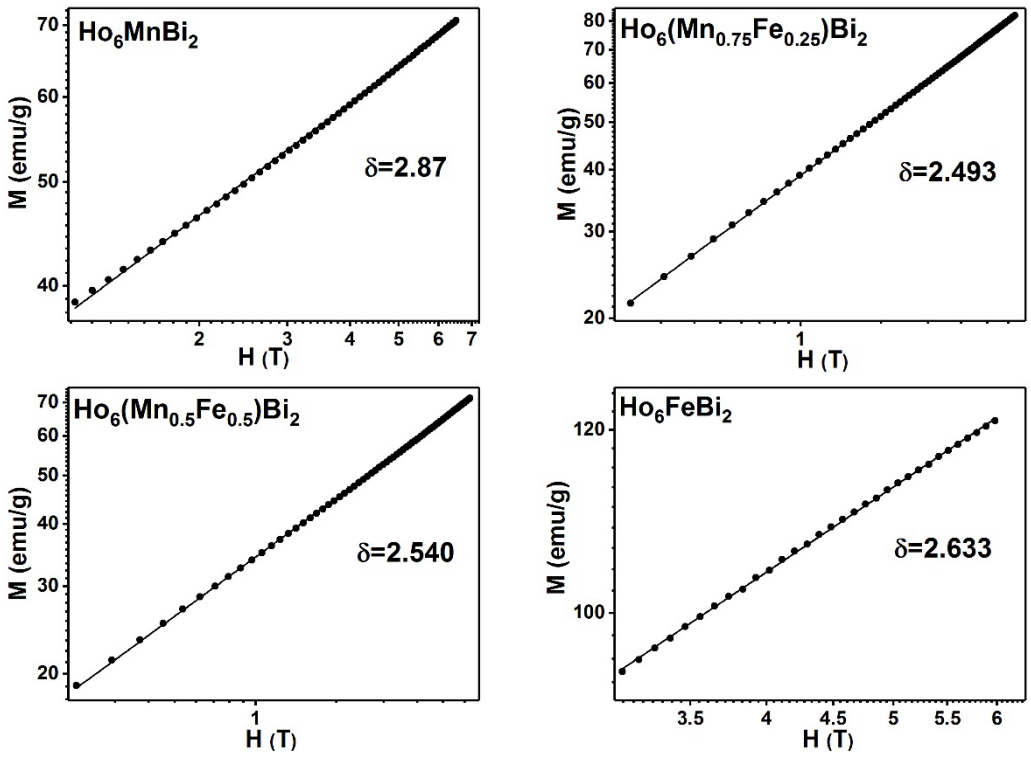


Fig. 7. *M* vs. *H* plot in a log-log scale collected at critical isotherms for the four compounds. The straight line, in each case, is the linear fit from which the exponent $\delta$ is obtained.

In order to further confirm a good scaling, $\beta$ and $\gamma$ values have been used to check the fulfilment of the magnetic equation of state Eq. (6), and the results are shown in Fig. 8. The collapse of the experimental data into two independent branches, above and below $T_C$, is extremely good in the four cases, which is generally taken as a severe confirmation of a proper scaling.

All these results indicate that the critical behavior of these transitions is close to the mean field universality class ($\beta_{theor} = 0.5$, $\gamma_{theor} = 1$, $\delta_{theor} = 3$) but with a deviation of the $\beta$ exponent which is not too strong for $Ho_6MnBi_2$ and $Ho_6FeBi_2$ (0.57 and 0.59, respectively) but gets farther away in the samples with shared Fe and Mn (0.68-0.69); $\gamma$,

on the other hand, keeps quite close to the theoretical value as it is between 0.99 and 1.13, while $\delta$ is slightly lower than the theoretical value (in the range 2.5-3).

In order to interpret these values, the possibility that the deviation from the mean field model is due to disorder in the system must be taken into account. There are two aspects which would indicate that disorder is present in the system and alters the critical behavior, the first one being the Harris criterion [43], i.e., the necessity for the critical exponent $\alpha$ to be positive. This is the critical exponent for specific heat, which can be calculated by means of the Rushbrooke's scaling law [29]:

$$\alpha + 2\beta + \gamma = 2, \tag{8}$$

But, for all cases, $\alpha$ is clearly negative; therefore, these transitions do not comply with the Harris criterion.

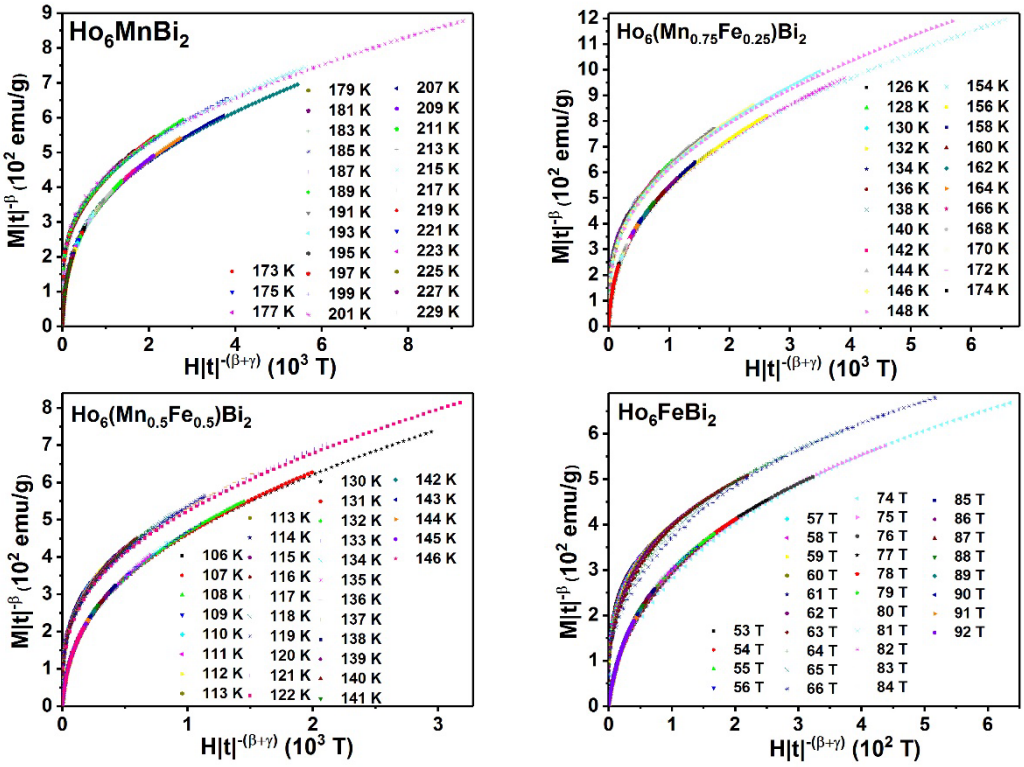


Fig. 8. The renormalized magnetization plotted as a function of the renormalized field following Eq. (6) for the four compounds. In each case, all data collapse in two separate branches, one above and one below the respective $T_C$.

Table 4. Critical exponents obtained for all compounds.

| Material | Technique | $\beta$ | $\gamma$ | $\delta$ |
|---|---|---|---|---|
| $Ho_6MnBi_2$ | Modified Arrott Plot | 0.591 ±0.002<br>$T_C$=204.11 ± 0.03 K | 1.125 ±0.005<br>$T_C$ =203.81 ± 0.05 K | 2.91[a] ± 0.01 |
| | Kouvel-Fisher Method | 0.566 ±0.008<br>$T_C$=203.71 ± 0.03 K | 1.13 ±0.01<br>$T_C$=203.75 ± 0.06 K | 3.00 [a] ± 0.05 |
| | Critical Isotherm | | | 2.87 ± 0.01 |
| $Ho_6(Mn_{0.75}Fe_{0.25})Bi_2$ | Modified Arrott Plot | 0.681 ±0.003<br>$T_C$=151.16 ± 0.02 K | 1.071 ±0.004<br>$T_C$=151.08 ± 0.04 K | 2.57 [a] ± 0.01 |
| | Kouvel-Fisher Method | 0.69 ±0.01<br>$T_C$=151.19 ± 0.03 K | 1.07 ±0.01<br>$T_C$=151.06 ± 0.06 K | 2.57 [a] ± 0.04 |
| | Critical Isotherm | | | 2.493 ± 0.003 |
| $Ho_6(Mn_{0.5}Fe_{0.5})Bi_2$ | Modified Arrott Plot | 0.690 ±0.004<br>$T_C$=126.04 ± 0.03 K | 1.103 ±0.009<br>$T_C$ =125.77 ± 0.07 K | 2.59[a] ± 0.02 |
| | Kouvel-Fisher Method | 0.68 ±0.01<br>$T_C$=125.94 ± 0.03 K | 1.09 ±0.03<br>$T_C$=125.82 ± 0.05 K | 2.609 [a] ± 0.07 |
| | Critical Isotherm | | | 2.540 ± 0.005 |
| $Ho_6FeBi_2$ | Modified Arrott Plot | 0.599 ±0.005<br>$T_C$=70.32 ± 0.03 K | 0.992 ±0.004<br>$T_C$ =70.16 ± 0.04 K | 2.66 [a] ± 0.02 |
| | Kouvel-Fisher Method | 0.59 ± 0.02<br>$T_C$=70.25 ± 0.03 K | 0.99 ±0.01<br>$T_C$=70.17 ± 0.07 K | 2.68 [a] ± 0.07 |
| | Critical Isotherm | | | 2.633 ± 0.009 |

[a] Calculated from Eq. (7) $\delta = 1 + \gamma/\beta$ .

The second issue is that, if disorder has altered the critical exponents, they should have a particular asymptotic behavior. The effective critical exponent $\gamma_{eff}$ is defined as

$$\gamma_{eff} = \frac{d(\ln \chi_0^{-1}(t))}{d(\ln t)} \tag{9}$$

It is well established that, in disordered magnets, $\gamma_{eff}$ will increase with the reduced temperature $t$ and present a well-defined maximum as we are getting farther away from the critical region, while in ordered ones it will have a monotonic behaviour [44-46]. $\gamma_{eff}$ values have been calculated as a function of $t$ and are shown in Fig. 9. Apart from some noise, the behavior does not match the properties related to disorder as there is no maximum as a function of $t$. Therefore, disorder is not responsible for the deviation from the mean field model.

Universality classes are theoretically developed on the basis of a particular Hamiltonian which takes into account particular mechanisms responsible for the magnetic interactions. More theoretical development from other groups in this field would be needed in order to account for deviations of the value of the critical exponent $\beta$ which will increase it, where disorder is not an issue, as it has been found in this work.

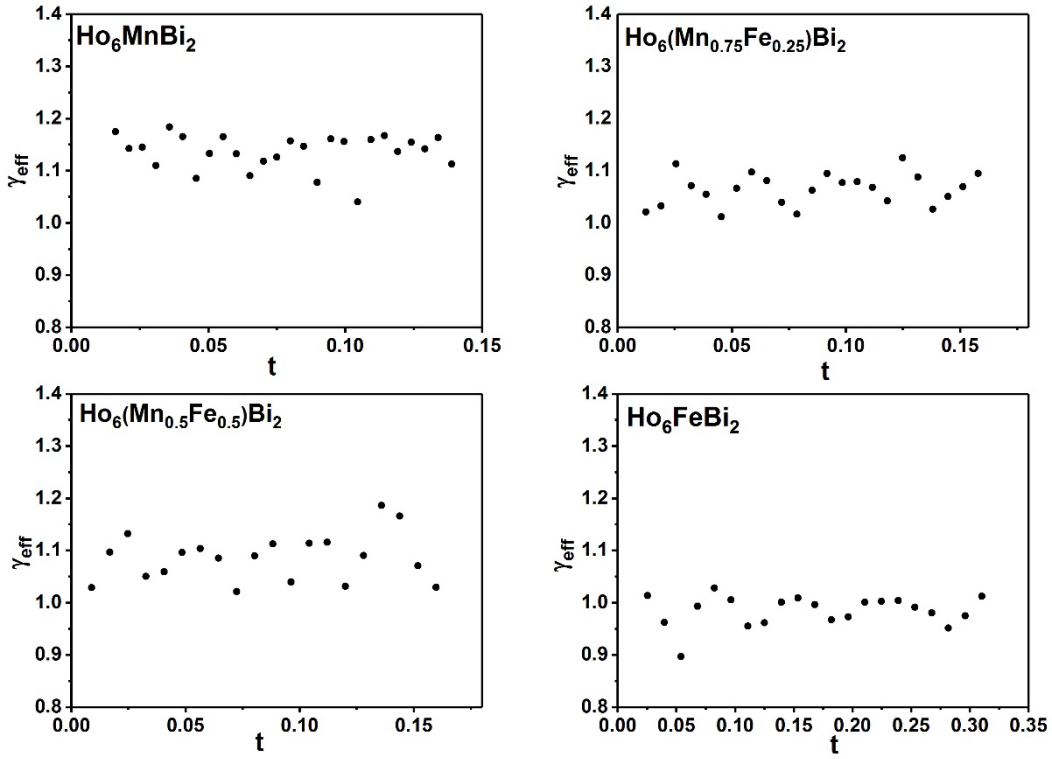


Fig. 9. Effective critical exponent $\gamma_{eff}$ for the four compounds as a function of the reduced temperature $t$.

### 3.2. Magnetocaloric properties

Concerning the magnetocaloric properties, Fig. 10 contains the entropy change as a function of temperature for different applied magnetic fields which has been calculated using Eq (1). The characterization of the magnetocaloric effect is done on the basis of the maximum value of the magnetic entropy change $\left|\Delta S_M^{pk}\right|$ for a given field and the refrigerant capacity (*RC*). The latter quantifies the energy transfer between the hot and cold reservoirs in a refrigeration cycle; therefore, for practical applications, a *RC* as large as possible over a wide range of temperatures is desirable. *RC* is usually calculated in two different (but equivalent) ways: $RC_{FWHM}$ is obtained multiplying the width of $\Delta S_M$ at half maximum times $\left|\Delta S_M^{pk}\right|$, while $RC_{AREA}$ is defined as the area enclosed by $\Delta S_M$ vs. temperature curves in the range enclosed by the full width at half maximum (FWHM). Both of them, together with the maximum of $\left|\Delta S_M^{pk}\right|$ for selected applied fields, are collected in Table 5. The applied fields have been chosen to match the ones generally reported in literature, 2 and 5 T, for a better comparison, also including the highest value measured, $\mu_0\Delta H$ = 6.9 T. At $\mu_0\Delta H$ = 2 T, $\left|\Delta S_M^{pk}\right|$ is given for the maximum around both $T_m$ and $T_C$ of each material, as well as the *RC* values, except in the case of $Ho_6FeBi_2$, where no *RC* values are given at $T_m$ because, as can be seen from Fig. 10d, there is not a clear maximum at that temperature and any attempt to calculate *RC* would give incorrect results. At 5 and 6.9 T the FWHM was calculated using the absolute maximum of the corresponding curve.

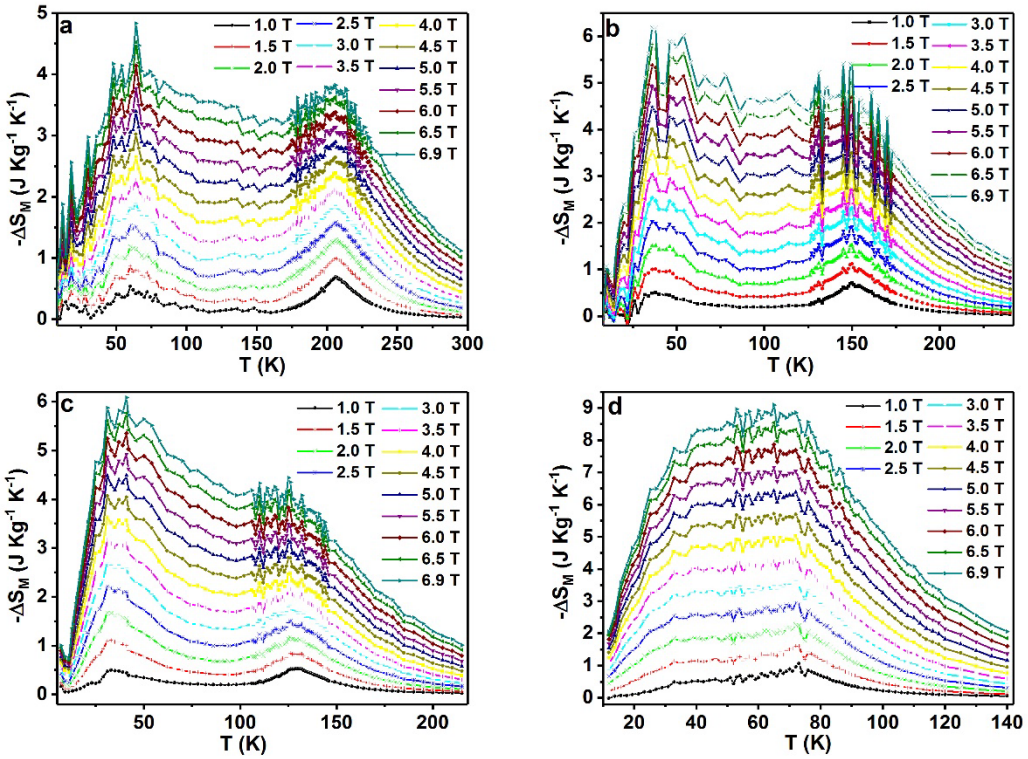


Fig. 10. Magnetic entropy change $-\Delta S_M$ for $\mu_0 \Delta H$ from 1 T to 6.9 T for: a) $Ho_6MnBi_2$, b) $Ho_6(Mn_{0.75}Fe_{0.25})Bi_2$, c) $Ho_6(Mn_{0.5}Fe_{0.5})Bi_2$, and d) $Ho_6FeBi_2$.

Table 5. Magnitude of the magnetic entropy change $\left|\Delta S_M^{pk}\right|$ and refrigerant capacities $RC_{FWHM}$ , $RC_{AREA}$ at different applied fields $\mu_0 \Delta H$ (2, 5 and 6.9 T) for the four compounds. The indicated temperatures correspond to the position of the maximum of $-\Delta S_M$.

| | | **Material** | | | |
|---|---|---|---|---|---|
| | | **$Ho_6MnBi_2$** | **$Ho_6(Mn_{0.75}Fe_{0.25})Bi_2$** | **$Ho_6(Mn_{0.5}Fe_{0.5})Bi_2$** | **$Ho_6FeBi_2$** |
| **2 T** | $\left\|\Delta S_M^{pk}\right\|$ **(J kg$^{-1}$ K$^{-1}$) [$T_m$]** | 1.2 (T = 60 K) | 1.5 (T = 38 K) | 1.7 (T = 31 K) | 1.8 (T = 33 K) |
| | $\left\|\Delta S_M^{pk}\right\|$ **(J kg$^{-1}$ K$^{-1}$) [$T_C$]** | 1.3 (T = 206 K) | 1.5 (T = 150 K) | 1.2 (T = 126 K) | 2.3 (T = 72 K) |
| | $RC_{FWHM}$ **(J kg$^{-1}$) [$T_m$]** | 73 (T = 60 K) | 80 (T = 38 K) | 81 (T = 31 K) | - |
| | $RC_{FWHM}$ **(J kg$^{-1}$) [$T_C$]** | 80 (T = 206 K) | 93 (T = 150 K) | 161 (T = 126 K) | 155 (T = 72 K) |
| | $RC_{Area}$ **(J kg$^{-1}$) [$T_m$]** | 54 (T = 60 K) | 61 (T = 38 K) | 61 (T = 31 K) | - |
| | $RC_{Area}$ **(J kg$^{-1}$) [$T_C$]** | 59 (T = 206 K) | 63 (T = 150 K) | 134 (T = 126 K) | 122 (T = 72 K) |
| **5 T** | $\left\|\Delta S_M^{pk}\right\|$ **(J kg$^{-1}$ K$^{-1}$) [$T_m$]** | 3.4 (T = 64 K) | 4.5 (T = 36 K) | 4.5 (T = 41 K) | 5.7 (T = 33 K) |
| | $\left\|\Delta S_M^{pk}\right\|$ **(J kg$^{-1}$ K$^{-1}$) [$T_C$]** | 2.9 (T = 206 K) | 3.9 (T = 150 K) | 3.2 (T = 125 K) | 6.4 (T = 72 K) |
| | $RC_{FWHM}$ **(J kg$^{-1}$)** | 709 (T = 64 K) | 691 (T = 36 K) | 569 (T = 41 K) | 520 (T = 65 K) |
| | $RC_{Area}$ **(J kg$^{-1}$)** | 508 (T = 64 K) | 506 (T = 36 K) | 506 (T = 41 K) | 434 (T = 65 K) |
| **6.9 T** | $\left\|\Delta S_M^{pk}\right\|$ **(J kg$^{-1}$ K$^{-1}$) [$T_m$]** | 4.8 (T = 64 K) | 6.2 (T = 36 K) | 6.1 (T = 41 K) | 7.7 (T = 33 K) |
| | $\left\|\Delta S_M^{pk}\right\|$ **(J kg$^{-1}$ K$^{-1}$) [$T_C$]** | 3.8 (T = 206 K) | 5.4 (T = 150 K) | 4.4 (T = 125 K) | 8.9 (T = 72 K) |
| | $RC_{FWHM}$ **(J kg$^{-1}$)** | 1020 (T = 64 K) | 979 (T = 36 K) | 801 (T = 41 K) | 777 (T = 65 K) |
| | $RC_{Area}$ **(J kg$^{-1}$)** | 738 (T = 64 K) | 743 (T = 36 K) | 730 (T = 41 K) | 633 (T = 65 K) |

Due to the subsequent phase transitions, the span in temperature of the full width at half maximum of these compounds is large, giving rise to huge *RC* values at high fields. Although the temperature span for the FWHM at $\mu_0\Delta H$ = 5 T decreases with Fe content, it is extremely broad: 209.0 K for $Ho_6MnBi_2$, 154.3 K for $Ho_6(Mn_{0.75}Fe_{0.25})Bi_2$, 126.7 K for $Ho_6(Mn_{0.5}Fe_{0.5})Bi_2$, and 80.9 K for $Ho_6FeBi_2$. Besides, the shapes of $\Delta S_M$ more and more tend to a plateau instead of the typical triangle, which is also interesting from the application point of view.

The highest $\left|\Delta S_M^{pk}\right|$ value at a given applied field is always given by $Ho_6FeBi_2$ and the lowest one by $Ho_6MnBi_2$, though the latter shows the biggest temperature span for high applied fields and the former the lowest one, which is translated into a higher *RC* value for the Mn sample over the Fe sample at 5 and 6.9 T. At lower fields, $\mu_0\Delta H$ = 2 T, when the *RC* value is given for $T_m$ and $T_C$, $Ho_6MnBi_2$ shows the lowest *RC* values. $Ho_6(Mn_{0.75}Fe_{0.25})Bi_2$ and $Ho_6(Mn_{0.5}Fe_{0.5})Bi_2$ samples present values in between the previously mentioned materials, which suggest the possibility of tuning the magnetocaloric effect by inserting different amount of Mn and Fe in the samples in order to search for the best applications, improving $\left|\Delta S_M^{pk}\right|$ or *RC*. Though the values of the peak entropy change are not high when compared with other rare-earth based magnetocaloric materials (see for instance Fig. 25 in [2]), the refrigerant capacity and the temperature span are considerably better than in most of them [2, 17, 19]. If we make the comparison with members of the $Ho_6TX_2$ family of compounds, there are published results for $Ho_6MnBi_2$ ($\left|\Delta S_M^{pk}\right|$=5 J kg$^{-1}$ K$^{-1}$ at $\mu_0\Delta H$ = 5 T and 215 K but the peak is only shown from 175 K upwards and no measurement of the refrigerant capacity is offered) [47] and $Ho_6CoTe_2$, but in this case the comparison is not worthy as the maxima for the entropy change are located at 60 K and 15 K [24]. There are also some results with a different rare earth such as $Tb_6FeX_2$ (X=Sb, Bi) [48] which give values of $\left|\Delta S_M^{pk}\right|$=2.25-2.67 J kg$^{-1}$ K$^{-1}$ at $\mu_0\Delta H$ = 5 T around 250 K, but without information about RC; or for $Gd_6FeBi_2$, with $\left|\Delta S_M^{pk}\right|$=4.3 J kg$^{-1}$ K$^{-1}$ at $\mu_0\Delta H$ = 5 T but it is displaced to a much higher temperature, around 350 K [49]. Finally, some other combinations are published, such as $Gd_6CoTe_2$ ($\left|\Delta S_M^{pk}\right|$=4.5 J kg$^{-1}$ K$^{-1}$ at 220 K and 6.5 J kg$^{-1}$ K$^{-1}$ at 180 K, all at 5 T, no information about RC) [25] or $Tb_6NiTe_2$ ($\left|\Delta S_M^{pk}\right|$=4.86 J kg$^{-1}$ K$^{-1}$ at 229 K at 5 T, no information about RC)

[50]. As a conclusion, the compounds studied in this work offer very good magnetocaloric properties within the general $R_6TX_2$ family over a broad temperature range.

In order to further study the magnetocaloric properties of this family, the next step is to build up the master curves of each compound for the transitions around $T_C$ following the method stablished in literature for second order phase transitions [26], which consists on normalizing the variation of the magnetic entropy change for each field with respect to the corresponding maximum value and rescaling the temperature axis. In ideal cases, one reference temperature $T_r$ is enough to obtain a good universal curve, where the scaling of the temperature axis is done in the following way:

$$\theta_1 = \frac{T - T_C}{T_r - T_C}. \tag{11}$$

$T_r$ is selected to be above $T_C$, corresponding to a certain fraction of $\left|\Delta S_M^{pk}\right|$; in our case, 0.5 has been used. Nevertheless, when the effect of the demagnetizing field is not negligible (which is the case), it is usually needed to use not one but two reference temperatures $T_{r1}$, $T_{r2}$ in order to construct the universal curves [27].

$$\theta_2 = \begin{cases} -(T - T_C)/(T_{r1} - T_C) & , \quad T \le T_C \\ (T - T_C)/(T_{r2} - T_C) & , \quad T > T_C \end{cases} \tag{12}$$

Fig. 11 shows the master curve for $Ho_6MnBi_2$ using one and two reference temperatures. It can be seen that, in the near vicinity of the critical temperature, different field curves overlap, confirming the second order character of the transition [28, 51]. When two reference temperatures are used to rescale the temperature axis the overlapping is even greater. At some point, for temperatures below $T_C$, the curves bend up, especially at higher fields. If in the region in which this methodology is applied there are other magnetic transitions, no overlapping is expected, as the present critical study is only valid for the PM-FM transition. Therefore, this deviation is due to the presence of the lower temperature transition, and it is responsible for the huge *RC* values and the flat central region of the magnetic entropy change. The effect is similar in the other three compounds.

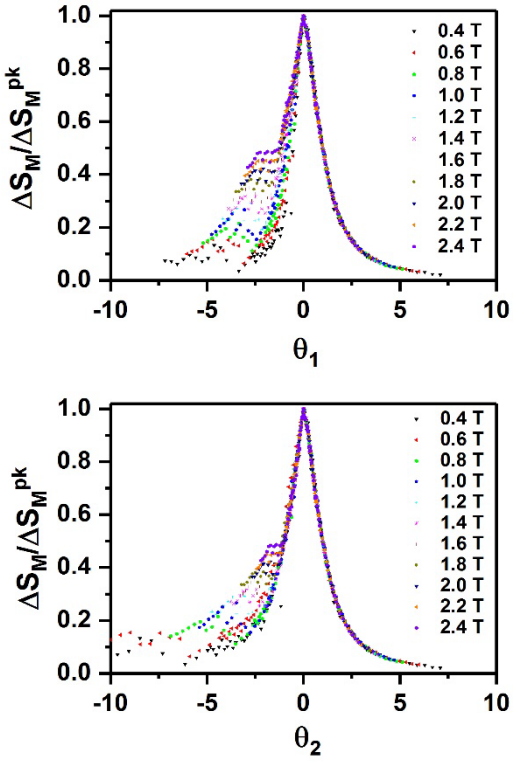


Fig. 11. Universal curve with the rescaled magnetic entropy changes for $Ho_6MnBi_2$ using one (upper box) or two (lower one) reference temperatures.

Finally, an interesting analysis is the study of the scaling of different magnetocaloric properties with the magnetic field, such as the maximum value of the magnetic entropy change $\left|\Delta S_M^{pk}\right|$ following Eq. (2) or the reference temperature $T_r$ which scales following the equation [26]:

$$T_r \propto H^{1/(\beta+\gamma)} \tag{13}$$

The previously obtained magnetic critical exponents $\beta$, $\gamma$ and $\delta$ have been used in order to check that both $\left|\Delta S_M^{pk}\right|$ and $T_r$ scale according to Eq. (2) and Eq. (13), respectively. As an example, Fig. 12 shows the scaling of the maximum variation of the magnetic entropy change for $Ho_6MnBi_2$ and $Ho_6(Mn_{0.5}Fe_{0.5})Bi_2$ and the scaling of the reference temperature for $Ho_6(Mn_{0.75}Fe_{0.25})Bi_2$ and $Ho_6FeBi_2$. The linear dependency confirms the obtained critical exponent values for the samples and, therefore, a correct scaling with the parameters previously found.

The scaling of the maximum value of the magnetic entropy change allows the extrapolation of this parameter to higher fields, which sometimes are not experimentally accessible, while the scaling of $T_r$, together with the universal curves, allows the

extrapolation of the whole magnetic entropy change curves to no accessible magnetic fields [44].

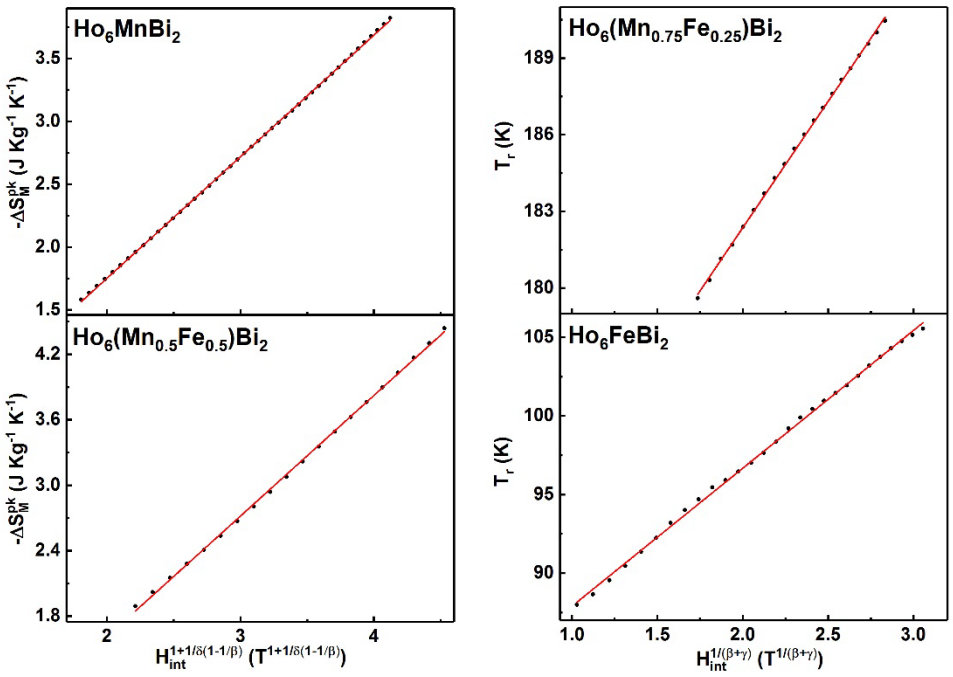


Fig. 12. Field dependences of the peak magnetic entropy change for some compounds (left). Scaling law for the reference temperature $T_r$ for some compounds (right). The values of $\beta$ and $\delta$ for each compound are the ones presented in Table 4.

## Conclusions

A very complete magnetic study has been performed in four compounds of the $Ho_6(Fe,Mn)Bi_2$ family, which have the peculiarity of presenting two magnetic transitions far apart. For each compound, the magnetocaloric effects, as well as the critical behavior of the PM-FM transition, have been studied in detail. The magnetic critical exponents $\beta$, $\gamma$ and $\delta$ have been obtained in near agreement with the Mean Field universality class, implying that the magnetic interactions are long-range. All of the compounds show relevant magnetocaloric properties over a very broad temperature range which links the two magnetic transitions: huge values of the refrigerant capacities (from 520 J/kg to 709 J/kg at 5T), good magnetic entropy changes (from 3.4 to 5.7 J/(kgK) at 5 T), a flat and wide temperature span for the working temperature range (nearly 200 K for the best case), making this family a promising candidate for refrigeration applications, and showing that these properties can be modified by appropriately tuning the composition. Using the

aforementioned critical exponents, the magnetocaloric scaling laws have been successfully tested and universal curves for the magnetic entropy change have also been obtained.

**Acknowledgements**

This work has been supported by Universidad del País Vasco UPV/EHU (GIU16/93). A. Herrero thanks the Department of Education of the Basque Government as grantee of the programme "Programa Predoctoral de Formación de Personal Investigador No Doctor". The authors thank for technical and human support provided by SGIker of UPV/EHU.

**References**

[1] A.M. Tishin, Y.I. Spichkin, *The Magnetocaloric Effect and its Applications*, Series in Condensed Matter Physics, Institute of Physics Publishing, Bristol and Philadelphia (2003).

[2] V. Franco, J.S. Blázquez, J.J. Ipus, J.Y. Law, L.M. Moreno-Ramírez, A. Conde, Magnetocaloric effect: *From materials research to refrigeration devices*, Prog. Mat. Sci. 93 (2018) 112-232.

[3] T. Gotschall, K.P. Skokov, M. Fries, A. Taubel, I. Radulov, F. Scheibel, D. Benke, S. Riegg, O. Gutfleisch, *Making a cool choice: The materials library of magnetic refrigeration*, Adv. Energy Mater. 9 (2019) 1901322 (1-13).

[4] L. Tocado, E. Palacios, R. Burriel, *Entropy determinations and magnetocaloric parameters in systems with first-order transitions: Study of MnAs*, J. Appl. Phys. 105 (2009) 093918.

[5] M. Balli, D. Fruchart, D. Gignoux, R. Zach, *The colossal magnetocaloric effect in $Mn_{1-x}Fe_xAs$: What are we really measuring?*, Appl. Phys. Lett. 95 (2009) 072509.

[6] A. Giguere, M. Foldeaki, B. Ravi Gopal, R. Chahine, T.K. Bose, A. Frydman, J.A. Barclay, *Direct measurement of the Giant adiabatic temperature change in $Gd_5Si_2Ge_2$*, Phys. Rev. Lett. 83 (1999) 2262-2265.

[7] J.D. Zou, B.G. Shen, B. Gao, J. Shen, J.R. Sun, *The magnetocaloric effect of $LaFe_{11.6}Si_{1.4}$, $La_{0.8}Nd_{0.2}Fe_{11.5}Si_{1.5}$, and $Ni_{43}Mn_{46}Sn_{11}$ compounds in the vicinity of the first-order transition*, Adv. Mater. 21 (2009) 693-696.

[8] G.J. Liu, J.R. Sun, J. Shen, B. Gao, H.W. Zhang, F.X. Hu, B.G. Shen, *Determination of the entropy changes in the compounds with a first-order magnetic transition*, Appl. Phys. Lett 90 (2007) 032507.

[9] V.K. Pecharsky, K.A. Gschneider, *Giant magnetocaloric effect in $Gd_5Si_2Ge_2$,* Jr. Phys. Rev. Lett. 78 (1997) 4494-4497.

[10] S. Couillaud, E. Gaudin, V. Franco. A. Conde, R. Pöttgen, B. Heying, U.Ch. Rodewald, B. Chevalier, *The magnetocaloric properties of GdScSi and GdScGe*, Intermetallics 19 (2011) 1573-1578.

[11] A. Herrero, A. Oleaga, P. Manfrinetti, A. Provino, A Salazar, *Study of the magnetocaloric effect in intermetallics RTX (R = Nd, Gd; T = Sc, Ti ; X = Si, Ge)*, Intermetallics 110 (2019) 106495.

[12] T. Krenke, E. Duman, M. Acet, E.F. Wassermann, X. Moya, L. Mañosa, A. Planes, *Inverse magnetocaloric effect in ferromagnetic Ni-Mn-Sn alloys*, Nat. Mater. 4 (2005) 450-454.

[13] F. Hu, B. Shen, J. Sun, *Magnetic entropy change in $Ni_{51.5}Mn_{22.7}Ga_{25.8}$ alloy*, Appl. Phys. Lett. 76 (2000) 3460-3462.

[14] Z.B. Guo, Y.W. Du, J.S. Zhu, H. Huang, W.P. Ding, D, Feng, *Large Magnetic Entropy Change in Perovskite-Type Manganese Oxides*, Phys. Rev. Lett. 78 (1997) 1142-1145.

[15] A. Fujita, S. Fujieda, Y. Hasegawa, K. Fukamichi, *Intinerant-electron metamagnetic transition and large magnetocaloric effects in $La(Fe_xSi_{1-x})_{13}$ compounds and their hydrides*, Phys. Rev. B 67 (2003) 104416.

[16] H. Wada, Y. Tanabe, *Giant magnetocaloric effect of $MnAs_{1-x}Sb_x$*, Appl. Phys. Lett 79 (2001) 3302-3304.

[17] H. Zhang, R. Gimaev, B. Kovalev, K. Kamilov, V. Zverev, *Review on the materials and devices for magnetic refrigeration in the temperature range of nitrogen and hydrogen liquefaction*, Phys. B: Condens. Matter 558 (2019) 65-73.

[18] H. Zhang, Y.J. Sun, E. Niu, L.H. Yang, J. Shen, F.X. Hu, J.R. Sun, B.G. Shen, *Large magnetocaloric effects of RFeSi (R = Tb and Dy) compounds for magnetic refrigeration in nitrogen and natural gas liquefaction*, Appl. Phys. Lett. 103 (2013) 202412.

[19] Y. Zhang, *Review of the structural, magnetic and magnetocaloric properties in ternary rare earth $RE_2T_2X$ type intermetallic compounds*, J. Alloys Compd. 787 (2019) 1173-1186

[20] S.A. Nikitin, A.S. Andreenko, A.M. Tishin, A.M. Arkharov, A.A. Zherdev, *Magnetocalorical effect in heavy rare earths*, Phys. Met. Metallogr. 60 (1985) 56.

[21] G. Green, W. Patton, J. Stevens, *The magnetocaloric effects of some rare earth metals*, Adv. Cryog. Eng. 33 (1988) 777-783.

[22] A.V. Morozkin, R. Nirmala, S.K. Malik, *Structural and magnetic properties of $Fe_2P$-type $R_6TX_2$ compounds (R=Zr, Dy, Ho, Er, T= Mn, Fe, Co, Cu, Ru, Rh, X=Sb, Bi, Te)*, Intermetallics 19 (2011) 1250-1264.

[23] A.V. Morozkin, *Magnetic structures of $Zr_6CoAs_2$-type $Ho_6FeSb_2$, $Ho_6CoBi_2$, $Ho_6FeBi_2$, $Ho_6MnBi_2$*, J. Alloys Compd. 395 (2005) 7-16.

[24] A.V. Morozkin, V.K. Genchel, A.V. Knotko, V.O. Yapaskurt, J. Yao, S. Quezado, S.K. Malik, *Structural and magnetic properties of $Fe_2P$-type $R_6TTe_2$ compounds (R=Tb,*

*Dy, Ho, Er, T= Fe, Co, Ru): Magnetic properties and specific features of magnetic entropy change*, J. Solid State Chem. 258 (2018) 201-211.

[25] A.V. Morozkin, YuMozharivskyj, V.Svitlyk, R.Nirmala, O.Isnard, P.Manfrinetti, A. Provino, C.Ritter, *Magnetic properties of $Fe_2P$-type $R_6CoTe_2$ compounds (R=Gd–Er)*, J. Solid State Chem. 183 (2010) 1314-1325.

[26] V. Franco, A. Conde, J.M. Romero-Enrique, J.S. Blázquez, *A universal curve for the magnetocalor effect: an analysis based on scaling relations,* J. Phys.: Condens. Matter 20 (2008) 285207 (5pp).

[27] V. Franco, J.S. Blázquez, A. Conde, *Field dependence of the magnetocaloric effect in materials with a second order phase transition: A master curve for the magnetic entropy change*, Appl. Phys. Lett. 89 (2006) 222512.

[28] C. Romero-Muñiz, R. Tamura, S. Tanaka, V. Franco, *Applicability of scaling behavior and power laws in the analysis of the magnetocaloric effect in second-order phase transition materilas*, Phys. Rev. B 94 (2016) 134401.

[29] H.E. Stanley, *Introduction to phase transitions and critical phenomena*, (1971) Oxford University Press.

[30] F. Izumi, *The Rietveld Method*, ed. by R.A. Young, Oxford University Press, Oxford, 1993, Chap. 13.

[31] H. Neves Bez, H. Yibole, A. Pathak, Y. Mudryk, V.K. Pecharsky, *Best practices in evaluation of the magnetocaloric effect from bulk magnetization measurements,* J. Magn. Magn. Mater. 458 (2018) 301–309.

[32] A.M. Tishin, *A review and new perspectives of the magnetocaloric effect: New materials and local heating and cooling inside the human body*, Int. J. Refrig. 68 (2016) 177-186.

[33] W. Jiang, X.Z. Zhou, G. Williams, Y. Mukovskii, K. Glazyrin, *Magnetic ground state and two-dimensional behavior in pseudo-kagome layered system $Cu_3Bi(SeO_3)_2O_2Br$*, Phys. Rev. B 78 (2008) 144409.

[34] W. Jiang, X.Z. Zhou, G. Williams, Y. Mukovskii, K. Glazyrin, *Coexistence of colossal magnetoresistance, a Griffiths-like phase, and a ferromagnetic insulating ground state in single crystal $La_{0.73}Ba_{0.27}MnO_3$*, Phys. Rev. B 77 (2008) 064424.

[35] A.V. Morozkin, Yu. Mozharivskyj, V. Svitlyk, R. Nirmala, S.K. Malik, *New ternary Yb5Sb3-type R5T1-x{Sb, Bi}2-x phases (R = Y, Dy, Ho, T = Co, Ru, Rh, Pd) and their magnetic properties*, Intermetallics 19 (2011) 302-306.

[36] J. Zhang, Y.M. Kang, G. Shan. S. Bobev, *Structural analysis of $Gd_6FeBi_2$ from single crystal X-ray diffraction methods and electronic structure calculations*, Acta Cryst. C75 (2019) 562-567.

[37] A.V. Morozkin, R. Nirmala, S.K. Malik, *Magnetic structure of the $Zr_6CoAs_2$-type $Er_6TX_2$ compounds (T= Mn, Fe, Co and X=Sb, Bi)*, J. Alloys Compd. 394 (2005) 75-79.

[38] S. Gupta, K.G. Suresh, *Review on magnetic and related properties of RTX compounds*, J. Alloys Compd. 618 (2015) 562-606.

[39] S.K. Banerjee, *On a generalised approach to first and second order magnetic transitions*, Phys. Lett. 12 (1964) 16.

[40] A.K. Pramanik, A. Banerjee, *Critical behavior at paramagnetic to ferromagnetic phase transition in $Pr_{0.5}Sr_{0.5}MnO_3$: A bulk magnetization study*, Phys. Rev. B 79 (2009) 214426.

[41] A. Oleaga, A. Salazar, M. Ciomaga Hatnean, G. Balakrishnan, *Three-dimensional Ising critical behavior in $R_{0.6}Sr_{0.4}MnO_3$(R=Pr,Nd) manganites*, Phys. Rev. B 92 (2015) 024409.

[42] J.S. Kouvel, M.E. Fisher, *Detailed Magnetic Behavior of Nickel Near its Curie Point*, Phys. Rev. 136 (1964) A1626.

[43] A.B. Harris, Journal of Physics C: Solid State Physics, *Effect of random defects on the critical behaviour of Ising models*, J. Phys. C 7 (1974) 1671 -1692.

[44] M. Fähnle, *Non-monotonic temperature dependence of the effective susceptibility exponent — A characteristic feature of many disordered spin systems*, J. Magn. Magn. Mater. 65 (1987) 1-6.

[45] M. Haug, M. Fähnle, H. Kronmüller, F. Haberey, *The magnetic phase transition in ordered and disordered ferrimagnets*, J. Magn. Magn. Mater. 69 (1987) 163-170.

[46] A. Perumal, V. Srinivas, *Quenched Disorder and the Critical Behavior of a Partially Frustrated System*, Phys. Rev. Lett. 91 (2003) 13.

[47] F. Wang, J. Zhang, F.Yuan, Y.Cao, C. Gao, Y. Hao, J. Shen, J. Sun, B. Shen, *Magnetic properties and magnetocaloric effect in $Ho_{6-x}Er_xMnBi_2$ compounds,* J. Appl. Phys. 107 (2010) 09A918.

[48] W. He, J. Zhang, L. Zeng, P. Qin, G. Cai, *Thermomagnetic properties near transitions of $Tb_6FeX_2$ (X = Sb, Bi)*, J. Alloys Compd. 443 (2007) 15-19.

[49] J. Zhang, G. Shan , Z. Zheng, C. H. Shek, *Structure and magnetic behaviors of $Gd_6FeBi_2$ compound*, Intermetallics 68 (2016) 51-56.

[50] A.V. Morozkin, Yu.Mozharivskyj, V.Svitlyk, R.Nirmala, A.K.Nigam, *Magnetic properties of $Fe_2P$-type $Tb_6FeTe_2$, $Tb_6CoTe_2$, $Tb_6NiTe_2$ and $Er_6FeTe_2$ compounds*, J. Solid State Chem. 183 (2010) 3039-3051.

[51] V. Franco, A. Conde, *Scaling laws for the magnetocaloric effect in second order phase transitions: From physics to applications for the characterization of materials*, Int. J. Refrig. 33 (2010) 465-473.